International Journal of Mathematical, Engineering and Management Sciences
Vol. 9, No. 5, 1035-1051, 2024
https://doi.org/10.33889/IJMEMS.2024.9.5.054

A Simple Online Tuning Flux Weighting Factor in Finite Control Set – Predictive Torque Control for Induction Motor Drive

Rozana Alik
Faculty of Electrical Engineering,
Universiti Teknologi Malaysia, Skudai, Johor, Malaysia.
E-mail: rozana91@graduate.utm.my

Shahrin Md Ayob
Faculty of Electrical Engineering,
Universiti Teknologi Malaysia, Skudai, Johor, Malaysia.
E-mail: e-shahrin@utm.my

Nik Rumzi Nik Idris
Faculty of Electrical Engineering,
Universiti Teknologi Malaysia, Skudai, Johor, Malaysia.
Corresponding author: nikrumzi@fke.utm.my

Norjulia Mohamad Nordin
Faculty of Electrical Engineering,
Universiti Teknologi Malaysia, Skudai, Johor, Malaysia.
E-mail: norjulia@utm.my

Mohammad Al Takrouri
Faculty of Electrical Engineering,
Universiti Teknologi Malaysia, Skudai, Johor, Malaysia.
E-mail: takrouri.moh@graduate.utm.my

Mohd Farid Muhamad Said
Institute of Vehicle Systems and Engineering (IVeSE),
Universiti Teknologi Malaysia, Skudai, Johor, Malaysia.
E-mail: mdfarid@utm.my

(Received on December 5, 2023; Received on March 26, 2024 & May 19, 2024 & June 12, 2024; Accepted on June 27, 2024)

Abstract
The Finite Control Set-Predictive Torque Control (FSC-PTC) is a practical and intuitive method to control an Induction Motor (IM). However, the challenge of this technique is the difficulty of tuning the weighting factor so that it performs optimally at all speeds. Hence, this paper proposes a new method for improving the optimization technique by automatically tuning the weighting factor using a flux controller. The flux controller is represented as a DC gain and designed to be proportional to the absolute value of the predicted stator flux error. This method eliminates the need for complex computation to select the suitable weighting factor while also efficiently regulating flux and torque. The proposed method is experimentally validated on a DS1104 controller board and compared to a constant flux weighting factor method that was tested under speed conditions. The results demonstrate that the new method can further decrease the torque ripple compared to the constant weighting factor while maintaining the flux ripple and harmonic distortion limits.

Keywords- Predictive control, Weighting factor (WF), Induction motor drive, dSPACE implementation.

1. Introduction

For decades, induction motors have been the workhorse of the industry. Its popularity is mainly due to its robustness, low maintenance costs, and its capability to operate at high speeds. Generally, the control of Induction Motor (IM) drives can be categorized into two types based on their applications; scalar control and vector control. Scalar control is commonly used in low- to medium-performance applications including pumps, fans, and compressors. For this type of application, regulating the steady-state speed is more critical than controlling the transient torque. The most common form of scalar control for IM applications is constant V/Hz control (Mahsahirun et al., 2020). Conversely, vector control is typically employed for high-performance applications that demand transient torque and speed control, such as traction drives, elevators, machine tools, and robotics. The advancements in high-performance IM drive control techniques are primarily attributed to improvements in power electronics converters and digital control techniques. The development of powerful and fast microprocessors and digital signal processors has also contributed to this progress. Control techniques that were not feasible for implementation decades ago can now be realized utilizing powerful processors, which are frequently paired with field-programmable gate arrays (FPGAs). Regardless of the implementation technique, minimizing sampling time is always desired to ensure a large control bandwidth.

Currently, the two most adopted control methods for high-performance IMs are Field-Oriented Control (FOC) and Direct Torque Control (DTC) (Trzynadlowski, 2000). Since its introduction in the early 1970s, FOC has been widely used in demanding applications involving torque control. It is highly sensitive to variations in motor parameters and requires precise knowledge of them to ensure accurate field orientation (Trzynadlowski, 2013). As it is dependent on current control, it requires a current control loop with a pulse width modulator, resulting in limited dynamic performance. In contrast, DTC offers a simpler structure and does not require a modulator or frame transformation. It was first presented in the late 1980s (Djamila and Yahia, 2020; Kang and Sul, 2001). However, the biggest flaw of DTC is its high torque and flux ripples. Over the last few decades, significant enhancements have been made to both FOC and DTC (Alsofyani et al., 2018; Bindal and Kaur, 2020; Peter et al., 2023; Wang et al., 2020), while concurrent research has also been conducted to develop superior control techniques.

A novel type of IM control technique based on Model Predictive Control (MPC) has recently been introduced (Abdelrahemet al., 2021; Elmorshedy et al., 2019; Mousavi et al., 2021). MPC was initially applied to slow-dynamical systems such as petrochemical industries, due to its substantial computing requirements. However, with the advancement of powerful processors, MPC applications for fast-dynamical systems such as power electronics converters and motor drives, are now viable. Among the many MPC variations that are applied in IM drive systems, Finite Control Set-Predictive Torque Control (FCS-PTC) has garnered remarkable attention due to its simplicity and ability to manage multiple constraints in one sampling period (Bordons and Montero, 2015; Geyer, 2017).

There are three main stages in FCS-PTC, namely: (i) stator flux estimation, (ii) stator flux and torque prediction, and (iii) cost function optimization (Rodriguez and Cortés, 2012). The third stage is selecting an optimal voltage vector (VV) for the inverter to minimize the cost function errors between predicted and reference torque and stator flux values. Since the torque and flux are fundamentally different in unit quantity, the weighting factor (WF) in the cost function is used to adjust the priorities between the torque and stator flux for VV selection. An incorrect value of WF may cause an imbalance in the IM's performance. For instance, if the flux WF is set to a high value, the flux control will be prioritized above the torque control, resulting in IMs having a smooth flux response but with a significant torque ripple. As a result, most FCS-PTCs that employ a constant WF may experience severe torque ripple at high speeds as well as poor steady-state performance at low speeds (Bhowate et al., 2019; Guazzelli et al., 2019). Therefore, optimizing the

WF value is vital to improve the IM's performance.

Early WF selection methods were time-consuming and reliant on heuristics (Cortés et al., 2009; Vazquez, et al., 2016). Next, researchers (Guazzelli et al., 2019; Zanchetta, 2011) suggested offline Multi-Objective Optimization (offline MOO) to improve the optimization technique. Nevertheless, it is still unable to achieve optimal WF and is dependent on specific operating conditions.

To address this issue, an online WF tuning method has been developed to automatically adapt the WF for each sampling period based on the motor's operating characteristics and performance requirements. (Davari et al., 2012) has presented a technique where the WF tuning depends on the torque vector instead of the magnitude. Unfortunately, it added complexity to the cost function. Furthermore, the authors (Bhowate et al., 2019; Ravi Eswar et al., 2018) have utilized the Multi-Criteria Decision-Making (MCDM) techniques in which the cost function is divided into three distinct parts based on the constraints. It will then be ranked and averaged once the minimum error of each cost function has been determined. Although this approach produced the ideal WF, it required additional optimization steps (Dragičević and Novak, 2019; Harbi et al., 2023; Novak et al., 2021).

Moreover, some researchers have completely removed the WF from the cost function. The authors in (Rojas et al., 2013; Rojas et al., 2015a; Rojas et al., 2015b; Tang et al., 2023; Tang et al., 2021) implemented the MOO methods too. Additionally, Parallel Predictive Torque Control (PPTC) with an adaptive selection method is proposed in (Wang et al., 2019). The authors of Zhang and Yang (2016) introduced an improved two-vector-based Model Predictive Torque Control (MPTC) method. Although the WF elimination approach is undoubtedly less complicated than the other approach, it is still unable to guarantee the best WF for the cost function. Rather, it has made computing times longer. Besides, certain researchers have proposed to use this method and make it simpler by reducing the utilization of VVs for the cost function (Mamdouh and Abido, 2019). Despite the efficiency and simplicity of this approach, this paper continues to incorporate the use of WF within the algorithm which focuses on enabling automatic real-time tuning of WF.

In addition, several researchers have utilized more intelligent techniques to improve cost function optimization such as Fuzzy Decision-Making (FDM) (Tang et al., 2021), VIKOR (Muddineni et al., 2016; Vujji and Dahiya, 2022), TOPSIS (Arshad et al., 2019; Muddineni et al., 2017) and Artificial Neural Networks (ANNs) (Vazquez et al., 2022). All these methods have undoubtedly been able to provide the optimal WF for the cost function unfortunately magnify both the complexity and computation time. **Table 1** summarizes the techniques that have been used to improve the optimization stage.

Therefore, this study proposes a straightforward and effective online WF tuning method that applies the flux controller (FC), where the predicted flux error is the basis of the generated WF. Additionally, this paper will include a detailed discussion on the effect of dynamic WF on IM performance. Hardware results have verified the efficiency of the proposed method's effectiveness, yielding little torque and flux ripples.

Section 2 of this work discusses the dynamic models of IM and Voltage Source Inverter (VSI). The third section presents the fundamental principle of FCS-PTC as well as the major problem of FCS-PTC when constant WF is utilized. Section 4 provides the methodology for designing the proposed improved FCS-PTC. Next, the experimental results are thoroughly discussed in Section 5. Lastly, Section 6 provides the conclusion for this research work.

Table 1. Summary of optimization improvement techniques.

Technique	Approach	Advantage (s)	Disadvantage (s)
With Weighting Factor	Empirical	Simple	Time consuming
	Offline multi objective optimization	Improve IM performance	Relies on specific operating points
	Online tuning		Complex and increase computational burden
	Multi criteria decision making		Relies on specific operating points
	Fuzzy Decision-Making		Complex and increase computational burden
	VIKOR and TOPSIS		
	Artificial Neural Network		
Without Weighting Factor	Multi objective optimization	Improve IM performance, reduce complexity	Increase computational burden
	Parallel Predictive Torque Control		
	Two vectors based MPTC		

2. Dynamic Model: Induction Motor and Voltage Source Inverter

To simplify the IM modelling, Equations (1) to (5) are used to quantify the stator voltage ($\boldsymbol{v}_s$), stator flux ($\boldsymbol{\psi}_s$), rotor flux ($\boldsymbol{\psi}_r$), and electromagnetic torque ($\boldsymbol{T}_e$) in a stationary reference frame for this research.

$$\boldsymbol{v}_s = \boldsymbol{i}_s R_s + d\boldsymbol{\psi}_s/dt \tag{1}$$

$$0 = \boldsymbol{i}_r R_r + d\boldsymbol{\psi}_r/dt - j\omega\boldsymbol{\psi}_r \tag{2}$$

$$\boldsymbol{\psi}_s = L_s\boldsymbol{i}_s + L_m\boldsymbol{i}_r \tag{3}$$

$$\boldsymbol{\psi}_r = L_r\boldsymbol{i}_r + L_m\boldsymbol{i}_s \tag{4}$$

$$\boldsymbol{T}_e = (3p/2)Im(\boldsymbol{i}_s\boldsymbol{\psi}_s^*) \tag{5}$$

where, R_s and R_r are the stator and rotor resistances. Meanwhile the stator and rotor current space vectors are represented as $\boldsymbol{i}_s$ and $\boldsymbol{i}_r$. Next, L_s, L_r and L_m indicate the stator self-inductance, rotor self-inductance and mutual inductance, respectively. Lastly, ω is the electrical rotor speed and the pole pairs is labelled as p.

The stator and rotor currents in Equations (6) and (7) can be obtained by manipulating Equations (3) and (4). The torque described in Equation (5), can be expressed in terms of d-axis and q-axis as shown in Equation (8).

$$\boldsymbol{i}_s = [1/(L_sL_r - L_m^2)]\,(L_r\boldsymbol{\psi}_s - L_m\boldsymbol{\psi}_r) \tag{6}$$

$$\boldsymbol{i}_r = [1/(L_sL_r - L_m^2)]\,(L_s\boldsymbol{\psi}_r - L_m\boldsymbol{\psi}_s) \tag{7}$$

$$T_e = (3p/2)\left[(\psi_{sd}i_{sq}) - (\psi_{sq}i_{sd})\right] \tag{8}$$

2.1 Three-Phase Voltage Source Inverter

This research employed a two-level, three-phase VSI. **Figure 1(a)** depicts the VSI configuration which comprises of six power Insulated Gate Bipolar Transistor (IGBT). Consequently, an eight switching states (S_A, S_B, and S_C) as presented in **Table 2**. Equation (9) depicts the stator voltage space vectors equation (Ghosh et al., 2019).

$$\boldsymbol{V_s} = \frac{2}{3}V_{DC}(S_A + \boldsymbol{a}S_B + \boldsymbol{a}^2S_C), \text{ where, } \boldsymbol{a} = e^{j\frac{2\pi}{3}} \text{ and } \boldsymbol{a}^2 = e^{j\frac{4\pi}{3}} \tag{9}$$

In this context, the switching state is designated as 1 when the top switch of a leg is activated, and 0 when the bottom switch is activated. **Figure 1(b)** displays six active VVs and two zero VVs on the d-q plane.

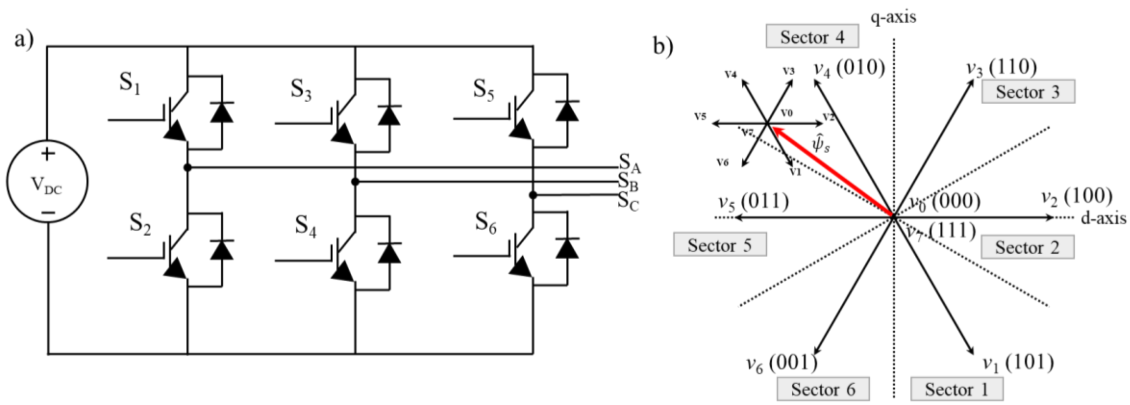

Figure 1. a) Three-phase VSI configuration and b) Voltage vectors on d-q plane.

Table 2. Voltage vectors for each switching state of 2L-VSI.

v_n	$s = [s_A s_B s_C]$	$v_s = v_d + jv_q$
v_0	0	0
v_1	101	$(1/3 - j\sqrt{3}/3)v_{DC}$
v_2	100	$(2/3)v_{DC}$
v_3	110	$(1/3 + j\sqrt{3}/3)v_{DC}$
v_4	010	$(-1/3 + j\sqrt{3}/3)v_{DC}$
v_5	011	$-(2/3)v_{DC}$
v_6	001	$(-1/3 - j\sqrt{3}/3)v_{DC}$
v_7	111	0

The optimization stage at FCS-PTC aims to select the VVs that minimize the ripple of torque and stator flux from their reference values. These VVs can be classified based on their contribution to either a more radial or tangential component relative to the circular flux locus. For instance, when the stator flux is located in Sector 3, v_3 and v_6 can be considered as VVs with high radial components, resulting in a greater impact on flux changes but a smaller impact on torque changes due to their small tangential components. At the same time, v_1, v_2, v_4, and v_5 have larger tangential components, which lead to a more significant influence on torque changes but a lesser effect on flux changes.

The impact of the zero VVs (v_0 and v_7) on torque changes is dependent on the motor speed. At lower speeds, applying zero VVs results in relatively minimal torque variations. However, as the speed increases, the effect on torque becomes more pronounced. In contrast, zero VVs have little effect on flux changes, regardless of speed. The optimization phase aims to select the VVs that minimize the deviation of torque and stator flux from their reference values.

3. FCS-PTC of Induction Motor

Figure 2 illustrates the schematic representation of the FCS-PTC of an IM. The FCS-PTC has three main stages (Rodriguez and Cortes, 2012): estimation, prediction, and optimization.

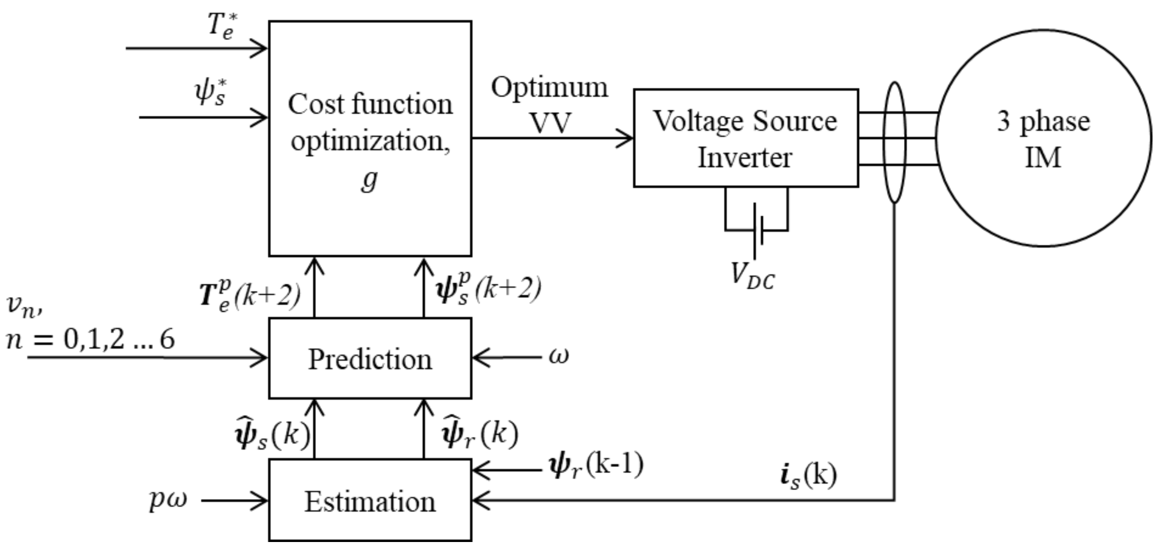

Figure 2. FCS-PTC block diagram with constant flux WF.

3.1 Estimation

This study estimates the stator flux using a current-based approach, which helps prevent the offset issue caused by inverter nonlinearities and current measurement error (Miranda et al., 2009). The rotor flux, $\hat{\boldsymbol{\psi}}_r$, is first computed using the rotor flux equation expressed in Equation (2) to estimate the stator flux. Equation (10) is the result of applying Euler discretization to formulate the equation.

$$\hat{\boldsymbol{\psi}}_r(k) = \hat{\boldsymbol{\psi}}_r(k-1) + T_s\left[R_r L_r L_m \boldsymbol{i}_s(k) - \left(1/(R_r L_r) - jp\omega\,(k)\right)\hat{\boldsymbol{\psi}}_r\,(k-1)\right] \tag{10}$$

where, T_s is sampling time. Then, the stator flux, $\hat{\psi}_s$ estimation is derived in Equation (11) by manipulating Equations (3) and (4)

$$\hat{\boldsymbol{\psi}}_s(k) = (L_m/L_r)\,\hat{\boldsymbol{\psi}}_r(k) + \boldsymbol{i}_s(k)\left(L_s - {L_m}^2/L_r L_s\right) \tag{11}$$

3.2 Prediction

This stage anticipates stator flux linkage ($\hat{\boldsymbol{\psi}}_s^p$) and the torque ($\boldsymbol{T}_e^p$) at $(k+1)$th. The stator flux prediction as in Equation (12) employs the forward Euler method based on Equation (1). To predict torque using Equation (5), stator current prediction is necessary, which is expressed in terms of estimated rotor flux linkage, measured stator current, and measured rotor speed. Consequently, utilizing Equations (12) and (13), the predicted torque is computed as Equation (14).

$$\boldsymbol{\psi}_s^p(k+1) = \hat{\boldsymbol{\psi}}_s(k) + T_s v_s - R_s \boldsymbol{i}_s(k) \tag{12}$$

$$\boldsymbol{i}_s^p(k+1) = (1 + T_s/\tau_\sigma)\boldsymbol{i}_s(k) + T_s/\tau_\sigma + T_s\left[1/R_\sigma\left[(k_r/\tau_r - k_r j\omega)\hat{\boldsymbol{\psi}}_r(k) + v_s(k)\right]\right] \tag{13}$$

$$\boldsymbol{T}_e^p(k+1) = 3p/2\ Im\left[\boldsymbol{\psi}_s^p(k+1)\boldsymbol{i}_s^p(k+1)\right] \tag{14}$$

where, τ_σ is the transient time constant of the stator, k_r is the rotor coupling factor and τ_r is the rotor time constant.

However, in the context of hardware implementation, a delay due to the sampling process is unavoidable.

Consequently, it becomes essential to introduce a delay compensation for the predicted torque and flux. This compensation can be attained by extrapolating the predictions of torque and flux to the next sampling time (k+2), utilizing the (k+1) values as the initial conditions. The resulting expressions for the predicted torque and flux are represented by Equations (15), (16) and (17), respectively.

$$\boldsymbol{\psi}_s^p(k+2) = \boldsymbol{\psi}_s^p(k+1) + T_s v_n - R_s \boldsymbol{i}_s^p(k+1) \tag{15}$$

$$\boldsymbol{i}_s^p(k+2) = (1 + T_s/\tau_\sigma)\boldsymbol{i}_s^p(k+1) + T_s/(\tau_\sigma + T_s)\left[1/R_\sigma\left[(k_r/\tau_r - k_r j\omega)\boldsymbol{\psi}_r^p(k+1) + v_s(k)\right]\right] \tag{16}$$

$$\boldsymbol{T}_e^p(k+2) = 3p/2\ Im\left[\boldsymbol{\psi}_s^p(k+2)\boldsymbol{i}_s^p(k+2)\right] \tag{17}$$

3.3 Optimization

The cost function identifies the optimal VV with the minimal error to be used as the subsequent switching state in the VSI. There are two main variables in the cost function: (i) predicted and reference values of the torque, and (ii) predicted and reference values of the stator flux. Thus, the cost function is defined as Equation (18).

$$g = \left|T_e^* - \boldsymbol{T}_e^p(k+2)\right| + \lambda_\psi\left|\psi_s^* - \boldsymbol{\psi}_s^p(k+2)\right| \tag{18}$$

where, the symbol (*) indicates the torque or flux as the reference value and λ_ψ is the flux weighting factor that determines the significance of the stator flux error relative to the torque error.

3.4 Major Problem in FCS-PTC with Constant WF

The FCS-PTC, which uses a fixed WF value, will not be able to adapt to changing operating conditions, potentially leading to performance issues in IM drives such as torque ripple at high speeds or flux errors at low speeds.

To illustrate this issue, a series of offline simulations were performed using MATLAB/Simulink. **Figure 3 3** shows the Simulink block diagram for the FCS-PTC IM drive utilized in the simulation. The control technique outlined in the previous part is only implemented for simulation purposes, exploiting the C S-function. The algorithm's sample time is set to 40 µs to match the hardware implementation. The simulation of the FCS-PTC drive was performed at three different speeds (30 rad/s, 80 rad/s, and 150 rad/s), with varying λ_ψ values ranging from 7 to 50. **Table 3** depicts the IM parameters used in the investigation. Equation (19) evaluates torque and flux ripples in terms of their standard deviation, σ, for each value of λ_ψ and speed.

$$\sigma_x = \sqrt{\sum|x - \bar{x}|^2/(n-1)} \tag{19}$$

In Equation (19), x is the flux or torque value of each sampling time, $\bar{x}$ is the sample mean, and n is the total number of data distributions. The results show the torque and flux ripples with different values of λ_ψ and speeds as shown in **Figure 4.**

Table 3. IM detailed parameters.

Parameter	Value	Parameter	Value
Rated power, P_{rated}	186 W	Rated torque, T_{rated}	1.25 Nm
Rated speed, ω_{rated}	150 rad/s	Rated flux, $\lvert\Psi\rvert_{rated}$	0.32 Wb
Stator resistance, R_s	9.9 Ω	Rotor resistance, R_r	8.15 Ω
Stator inductance, L_s	0.2786 H	Rotor inductance, L_r	0.2853 H
Magnetizing inductance, L_m	0.2651 H	Pole pairs	2

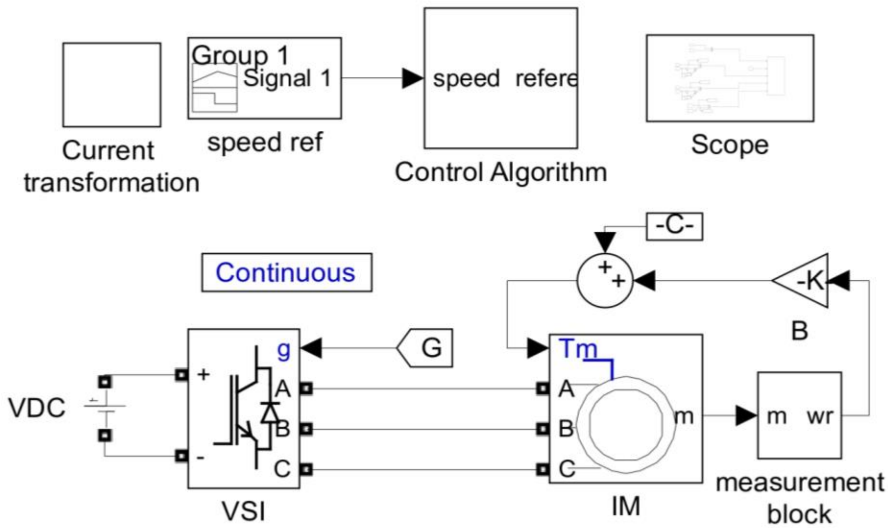

Figure 3. Complete simulation block diagram.

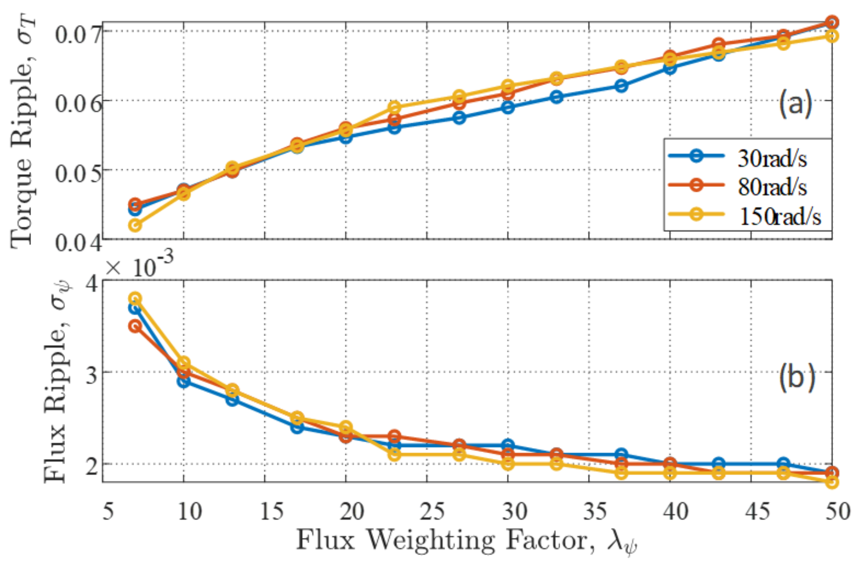

Figure 4. Torque and flux ripples with different flux weighting factors.

In **Figure 4(a)**, the data reveal that as the parameter λ_ψ increases, torque ripple (σ_T) exhibits an increase, while lower values of λ_ψ correspond to the lowest σ_T. In contrast, **Figure 4(b)** demonstrates that lower λ_ψ values result in significant flux ripple (σ_ψ), whereas higher λ_ψ values provide low σ_ψ but yield high σ_T. Moreover, it is seen that high-speed condition produces the highest σ_T with an average σ_T value of 0.0591. Conversely, the highest σ_ψ value, averaging at 0.00234, occurs when the speed is at 30 rad/s (low-speed condition). This emphasizes the priority of flux control at lower speeds and torque control at higher speeds. Besides, it is evident that minimizing σ_ψ helps to ensure the σ_T in an acceptable range. However, it is not applicable for the opposite situation. This highlights the importance of selecting an appropriate λ_ψ value for each speed condition to minimize both σ_T and σ_ψ.

As discussed in the literature review (Section 1), existing WF selection methods are often complex and computationally intensive; they are either performed offline or online. In response to these challenges, this paper presents a straightforward online tuning method based on predicted stator flux error. Unlike the previous methods, no heavy computational requirement is needed thus ensuring a small sampling time and hence larger control bandwidth.

4. Proposed FCS-PTC

The proposed method, illustrated in **Figure 5**, utilizes a FC to dynamically determine the value of WF based on the absolute predicted flux error ($|\Delta\psi|^p$) between the reference and predicted stator flux values. In this work, FC is represented as a DC gain, k_{fc}. As $|\Delta\psi|^p$ increases, a higher value of WF should be obtained to emphasize the importance of flux control. Subsequently, the cost function will choose the VVs that prioritize flux control to reduce the flux ripple.

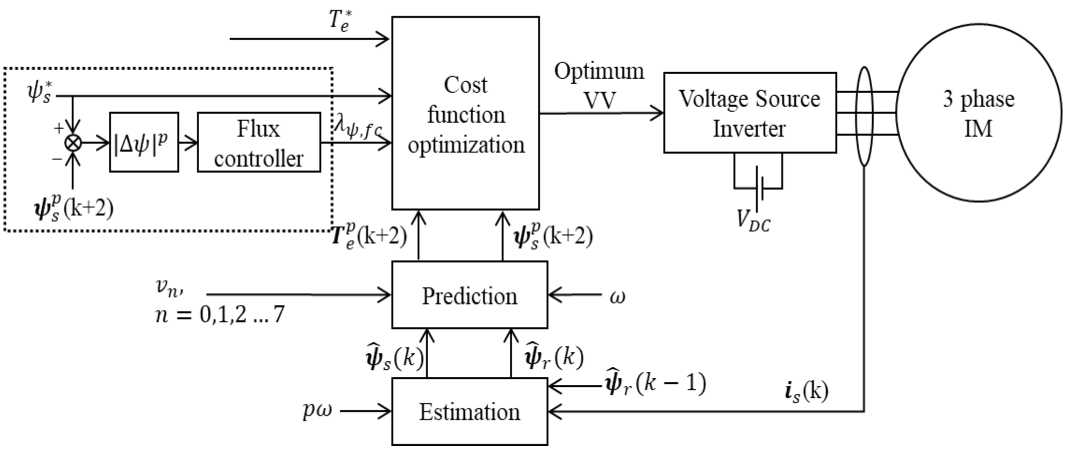

Figure 5. Proposed FCS-PTC with flux controller.

It must be highlighted that the role of FC or the k_{fc} is not to eliminate or minimize flux ripple, as this task is dependent on the VVs selection by the cost function. Rather, the FC is used to ensure a fast dynamic WF response to generate an appropriate value of WF, directly proportional to the $|\Delta\psi|^p$.

If the absolute predicted flux error and predicted torque error are defined by Equations (20) and (21), respectively, then the cost function in Equation (18) using a constant λ_ψ, can be written as Equation (22).

$$|\Delta\psi|^p = \left|\,\psi_s^* - \boldsymbol{\psi}_s^p(k+2)\right| \tag{20}$$

$$|\Delta T|^p = \left|T_e^* - \boldsymbol{T}_e^p\,(k+2)\,\right| \tag{21}$$

$$g = |\Delta T|^p + \lambda_\psi |\Delta\psi|^p \tag{22}$$

Meanwhile, the dynamic WF, denoted as $\lambda_{\psi,fc}$ for proposed method in **Figure 5** can be determine as k_{fc} multiply with $|\Delta\psi|^p$. Hence, the new cost function, g_{fc} for the suggested method can be written as Equation (23). By comparing Equations (22) and (23), the value of k_{fc} can be determine as Equation (24).

$$g_{\mathrm{fc}} = |\Delta T|^p + k_{\mathrm{fc}}(|\Delta\psi|^p)^2 \tag{23}$$

$$k_{\mathrm{fc}} = \lambda_{\psi nominal}/|\Delta\psi_{TH}| \tag{24}$$

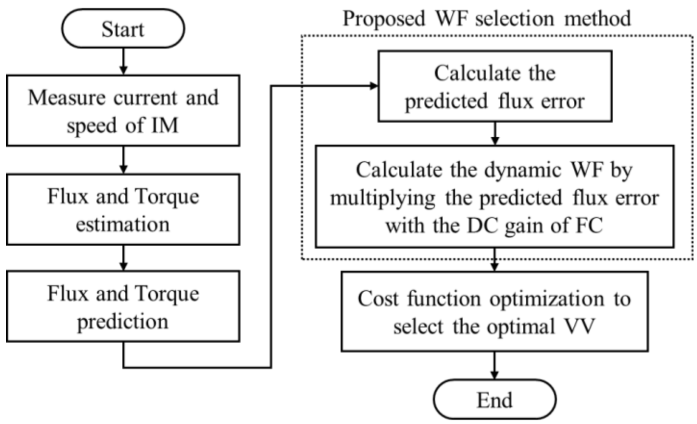

Figure 6. Flowchart of the proposed method.

To facilitate the selection of the value for k_{fc}, it is crucial to identify one significant parameter, which is defined as the absolute threshold predicted flux error, denoted as $|\Delta\psi_{TH}|$, as shown in Equation (25). The term $|\Delta\psi_{TH}|$ refers to a maximum permitted flux error that determines the value k_{fc} for a specific value of $\lambda_{\psi nominal}$. The value of $\lambda_{\psi nominal}$ will be selected from the offline experiments that provide a considerable low flux and torque ripple. Furthermore, according to (Zhong et al.,1997), the optimal flux hysteresis bandwidth should be 5% of the rated flux, which results in optimal harmonic distortion and optimal switching frequency. In this research, the threshold is set to be 2%, which is less than half of 5%. Consequently, a threshold predicted flux error of 0.0064 is selected in this work, which corresponds to 2% of the reference flux of 0.32 Wb. **Figure 6** is presented to provide more insight on the proposed improved FCS-PTC method.

5. Experimental Results

Figure 7 shows the experimental validation of the suggested technique using a 186 W, 1425 RPM, 3-phase IM drive fed by a 2-level VSI. **Table 3** includes detailed parameters for the IM. The algorithm is then fully programmed onto the DS1104 controller board.

Generally, programming the DS1104 can be done in two ways. The first way entails developing the control algorithm using SIMULINK. The algorithm is subsequently compiled and uploaded into the DS1104 for real-time execution. It is the simplest and quickest approach of programming. The second way is more manual which involves writing C programs known as hand coding. This is accomplished by calling C functions from dSPACE's real-time library. The C codes are then compiled, linked, and loaded into the DS1104. The second procedure takes longer and is more tedious than the first. However, when it comes to complex control algorithms like FCS-PTC, the second method is often the best option. Hand-coded C programmes allow for a sample time of 40 µs, which is not possible with SIMULINK.

To accurately monitor and measure the motor speed, an incremental speed encoder with 2048 pulses per revolution sampled at 0.001s was used. Two-phase currents of the IM were sensed using two current sensors. Simultaneously, the switching pulses were generated by the DS1104 Slave DSP PWM3 Duty.

Based on the offline experiment, the $\lambda_{\psi\mathrm{nominal}}$ is selected to be 17. With the $|\Delta\psi_{TH}|$ equal to 0.0064 and using Equation (24), the value of k_{fc} is calculated to be 2656.25. Thus, in this paper, a comparison is made between two methods: the proposed FCS-PTC and the FCS-PTC with constant WF, λ_{ψ} value of 17.

1.15.1 Speed Reversal Performance

Figure 8 illustrates the IM response to speed reversals. This figure demonstrates excellent dynamic performances for both methods, whereby the speed rapidly reverses from 100 rad/s to -100 rad/s in less than 0.2s. This observation suggests that the dynamic performance of both techniques is similar and comparable.

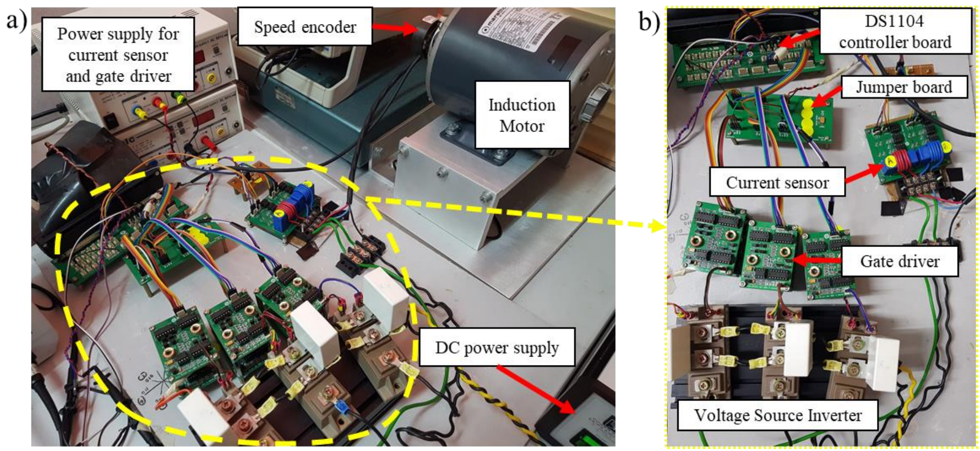

Figure 7. Experimental set-up.

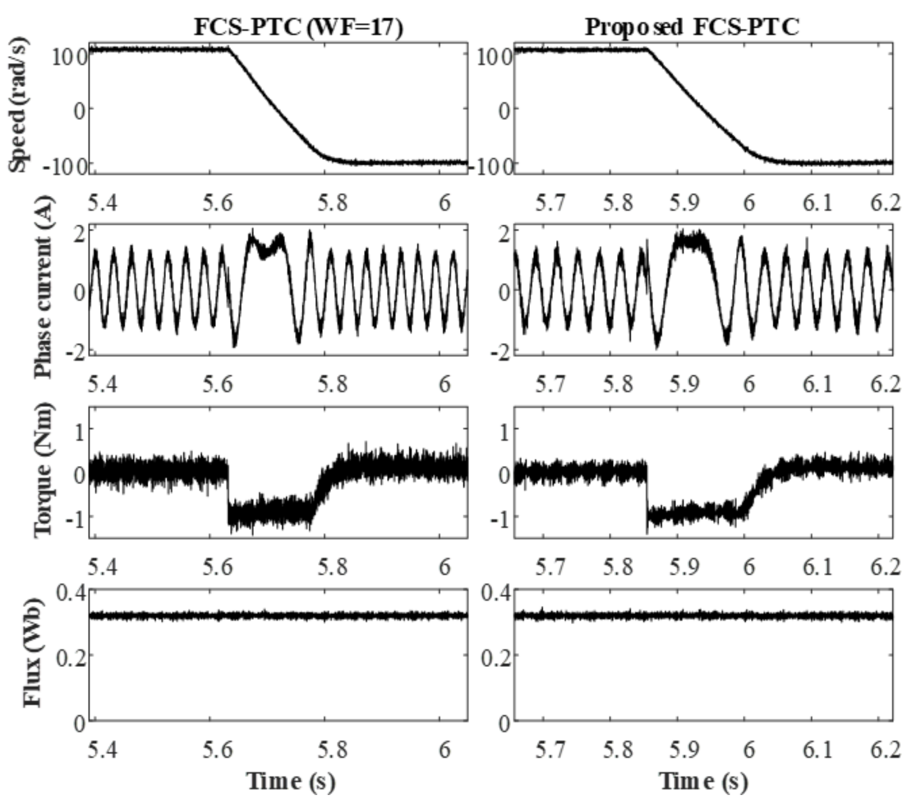

Figure 8. Speed, torque, stator flux, and stator current during speed reversal for the constant WF (left) and proposed (right) methods.

5.2 Steady State Performance

Next, a steady-state evaluation is performed to assess the advantages and drawbacks of both methods. This analysis specifically considers current, torque, and flux, encompassing three different speed conditions: 30 rad/s (low), 80 rad/s (medium), and 150 rad/s (high), as illustrated in **Figure 9, 10, and 11**.

From the three figures, it can be seen that the proposed method has been able to provide dynamic changes in flux WF, λ_ψ for every speed condition in every sampling period. The current and flux performances of both methods exhibit almost identical results across all speed conditions. This is valid because theoretically, the current performance is mainly influenced by the flux performance (Casadei et al., 1994). This result aligns with expectations since the proposed method utilizes λ_ψ of 17 as the reference; hence, the flux performance should be similar. As a result, at λ_ψ of 17, the σ_ψ and current harmonic ought to be almost identical to the σ_ψ. Nonetheless, **Figures 9, 10, and 11** demonstrate a discernible improvement in torque performance for the proposed method. This improvement is consistent with the inference drawn in Section 3.4, which emphasizes that under all speed conditions, minimizing σ_ψ aids in minimizing σ_T.

To provide more insights, **Table 4** presents a comprehensive overview of the results for harmonic current, σ_T, and σ_ψ. The current harmonic measurements were obtained using FFT analysis in MATLAB/Simulink, with a maximum frequency of up to 10,000 Hz. **Table 4** shows that at all speeds, σ_T has decreased by at least 3.22%. Meanwhile, there is less than a 2% difference between the σ_ψ for the proposed and the constant WF method, which stays almost the same. The proportion of current distortion, where the average disparity is 0.54%, exhibits a similar pattern. This is to be expected, as the current distortion is mainly influenced by the flux response instead of the torque response, as mentioned earlier.

Figure 12 illustrates the distribution of frequencies for the parameterλ_ψ. Observably, the proposed method used high values of λ_ψ (those exceeding 60) at low speeds of 30 rad/s. On the other hand, a higher number of low λ_ψ values (those less than 20) are employed at higher speeds. This suggests that the proposed technique effectively satisfies the requirement to prioritize torque control at higher speeds while emphasizing greater flux control at lower speeds.

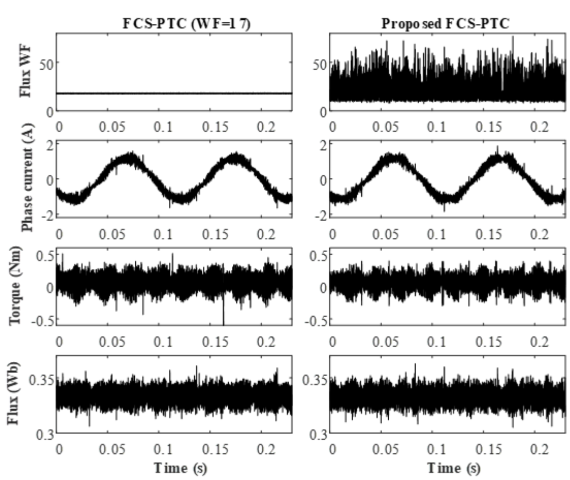

Figure 9. Phase current, torque and flux response at 30rad/s for constant WF (left) and proposed (right) method.

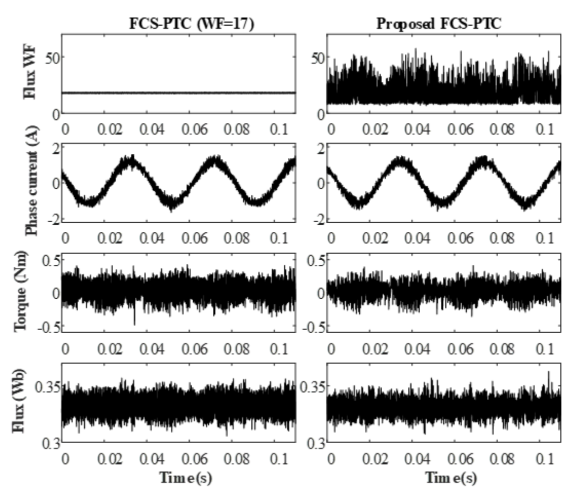

Figure 10. Phase current, torque and flux response at 80rad/s for constant WF (left) and proposed (right) method.

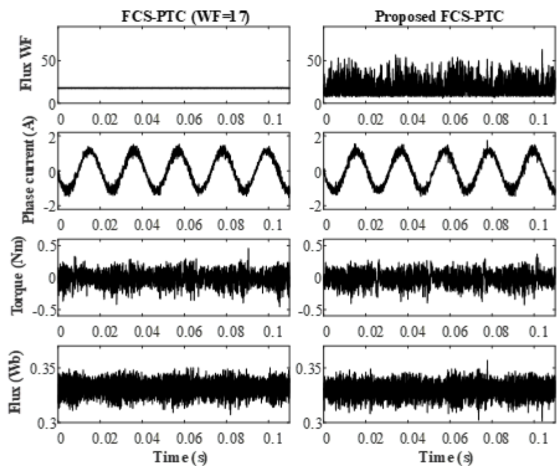

Figure 11. Phase current, torque and flux response at 150rad/s for constant WF (left) and proposed (right) method.

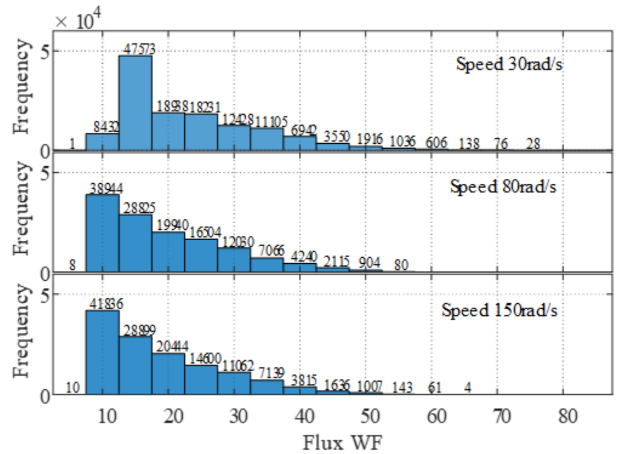

Figure 12. Frequency distribution for flux weighting factor.

Table 4. Torque ripple, flux ripple and current harmonic for both methods.

Speed (rad/s)	Torque ripple, σ_T			Flux ripple, σ_ψ			Current harmonic (%)		
	Constant WF	Proposed	% different	Constant WF	Proposed	% different	Constant WF	Proposed	% different
30	0.1003	0.0954	-4.89	0.0052	0.0053	+1.92	14.01	14.11	+0.73
80	0.1118	0.1082	-3.22	0.0058	0.0058	0	15.98	16.00	+0.13
150	0.1025	0.0991	-3.32	0.0053	0.0054	+1.89	15.78	15.90	+0.76

5.3 Voltage Vector Analysis

VV analysis is performed for the three speeds conditions to deepen the understanding of how the proposed method, with dynamic λ_ψ values, can improve flux and torque control. **Figure 13** depicts the selected VVs when the flux is in Sector 3 (shown in **Figure 1(b)**) at low, medium, and high speeds, respectively.

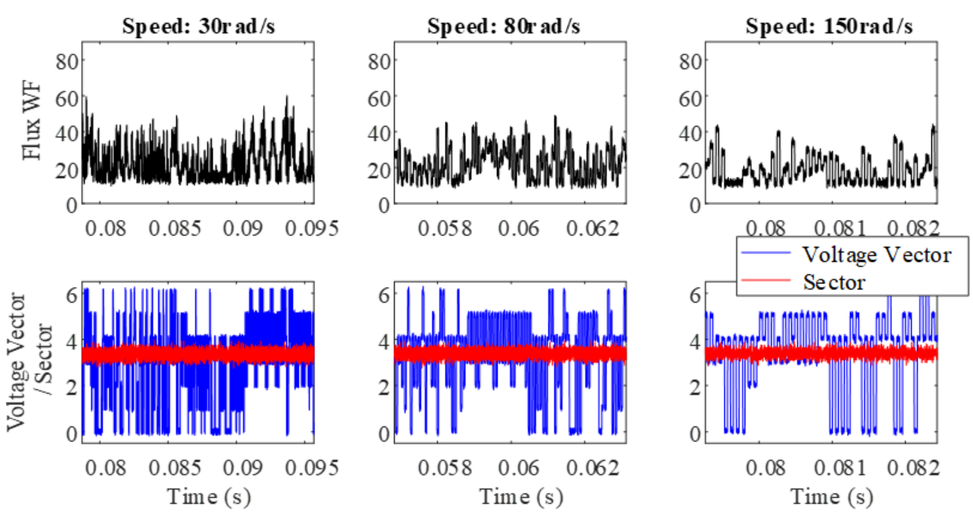

Figure 13. Voltage vector and selected flux weighting factor at sector 3.

Figure 13 showcases that at lower speeds, flux control is more critical than torque control. This leads to a preference for higher λ_{ψ} values. Consequently, the radial VVs, v_3 and v_6 options are less favored as they induce significant changes to the flux and will cause distortion. Therefore, the tangential VVs, v_4 and v_5 are preferred due to their minimal impact on flux at lower speeds. Additionally, even the zero voltage vectors (zero VVs) are chosen because they also result in minimal flux changes.

As speed increases, torque control becomes more prominent, hence smaller λ_{ψ} is desirable. Notably, zero VV is used less commonly since it produces considerable torque changes. Tangential VVs, such as v_4 and v_5 , become the dominant torque control options at higher speeds. Occasionally, the radial component vectors like v_3 and v_6 are also selected for torque and flux control. All these results align with the theory stated in Section 2.1.

6. Conclusion

A straightforward and effective technique is presented for real-time adjustment of a WF in an FCS-PTC IM drive. The novelty of this research lies in the innovative approach to tune the WF, which has been a significant challenge in the field. There are four key points highlighting the novelty of the work:

(i) The research introduces a FC to provide dynamic fast WF tuning response for the FCS-PTC.
(ii) The FC enables automatic tuning of the WF, a significant improvement over manual tuning or using constant WF.
(iii) The proposed method uses simple mathematical method which removes the need for complex computation in selecting the WF.
(iv) This research includes experimental validation using DS1104 controller board and the outcomes substantiate the effectiveness of the suggested method in enhancing the performance of the IM.

Based on experimental results, it reveals that the FCS-PTC with the constant WF method may reduce σ_{ψ} with increased σ_T, particularly at high speeds. In contrast, the proposed method effectively preserves flux performance while displaying minimal current distortions. The difference in flux does not exceed 0.0001 Wb. Furthermore, the proposed method significantly reduces torque ripple by a range of 3% to 5% compared to the FCS-PTC with the constant WF method. It is anticipated that by implementing the proposed improved FCS-PTC method, the overall IM performance and efficiency will be enhanced. The IM can be used for a longer duration, as there will be no unwanted heat generation caused by the high flux ripple and high current distortions, as well as no unnecessary vibration due to the high torque ripple.

Furthermore, several recommendations for future work can be made for this research. For example, the suggested approach can be applied to an IM with a higher power rating. In addition, the IM can be connected to any active load to study how the proposed method performs under the added complexity introduced by the load. A larger motor generates a larger torque, allowing for a more comprehensive transient state analysis. The proposed method can be implemented and analysed in the flux weakening region, which is typically where the motor operates at speeds higher than the rated speed. Analysing the proposed method in this region can provide insights into the system's overall performance and verify if the proposed method meets its intended performance targets. It also helps to identify any potential issues or limitations of the proposed method.

Conflict of Interest

The authors confirm that there is no conflict of interest to declare for this publication.

Acknowledgments

This work was supported by the Ministry of High Education and Universiti Teknologi Malaysia under Flagship CoE/RG Grant (Vot 477 no. 10G13). The authors extend their appreciation to Intelligent Prognostic Private Limited Delhi, India; for providing technical and non-technical support in this research work. The authors also would like to thank the editor and anonymous reviewers for their comments that helped improve the quality of this work.

References

Abdelrahem, M., Hackl, C.M., Kennel, R., & Rodriguez, J. (2021). Computationally efficient finite-position-set-phase-locked loop for sensorless control of PMSGs in wind turbine applications. *IEEE Transactions on Power Electronics, 36*(3), 3007-3016. https://doi.org/10.1109/tpel.2020.3015575.

Alsofyani, I.M., Idris, N.R.N., & Lee, K.B. (2018). Dynamic hysteresis torque band for improving the performance of lookup-table-based DTC of induction machines. *IEEE Transactions on Power Electronics, 33*(9), 7959-7970. https://doi.org/10.1109/tpel.2017.2773129.

Arshad, M.H., Abido, M.A., Salem, A., & Elsayed, A.H. (2019). Weighting factors optimization of model predictive torque control of induction motor using NSGA-II with TOPSIS decision making. *IEEE Access, 7*, 177595-177606. https://doi.org/10.1109/access.2019.2958415.

Bhowate, A., Aware, M., & Sharma, S. (2019). Predictive torque control with online weighting factor computation technique to improve performance of induction motor drive in low speed region. *IEEE Access, 7*, 42309-42321. https://doi.org/10.1109/access.2019.2908289.

Bindal, R.K., & Kaur, I. (2020). Torque ripple reduction of induction motor using dynamic fuzzy prediction direct torque control. *ISA Transactions, 99*, 322-338. https://doi.org/10.1016/j.isatra.2019.09.012.

Bordons, C., & Montero, C. (2015). Basic principles of MPC for power converters: Bridging the gap between theory and practice. *IEEE Industrial Electronics Magazine, 9*(3), 31-43. https://doi.org/10.1109/mie.2014.2356600.

Casadei, D., Grandi, G., Serra, G., & Tani, A. (1994). Effects of flux and torque hysteresis band amplitude in direct torque control of induction machines. In *Proceedings of IECON'94-20th Annual Conference of IEEE Industrial Electronics* (Vol. 1, pp. 299-304). IEEE. Bologna, Italy. https://doi.org/10.1109/iecon.1994.397792.

Cortés, P., Kouro, S., La Rocca, B., Vargas, R., Rodríguez, J., León, J.I., Vazquez, S., & Franquelo, L.G. (2009). Guidelines for weighting factors design in model predictive control of power converters and drives. In *2009 IEEE International Conference on Industrial Technology* (pp. 1-7). IEEE. Churchill, VIC, Australia. https://doi.org/10.1109/icit.2009.4939742.

Davari, S.A., Khaburi, D.A., & Kennel, R. (2012). An improved FCS-MPC algorithm for an induction motor with an imposed optimized weighting factor. *IEEE transactions on Power Electronics, 27*(3), 1540-1551. https://doi.org/10.1109/tpel.2011.2162343.

Djamila, C., & Yahia, M. (2020). Direct torque control strategies of induction machine: Comparative studies. In Salem, F.B. (ed) *Direct Torque Control Strategies of Electrical Machines* (pp. 17-42). Intech Open. https://www.intechopen.com/books/8686.

Dragičević, T., & Novak, M. (2019). Weighting factor design in model predictive control of power electronic converters: An artificial neural network approach. *IEEE Transactions on Industrial Electronics, 66*(11), 8870-8880. https://doi.org/10.1109/tie.2018.2875660.

Elmorshedy, M.F., Xu, W., Liu, Y., Allam, S.M., & Dong, M. (2019). Speed control of linear induction motor based on finite-set model predictive direct flux control. In *2019 IEEE International Symposium on Predictive Control of Electrical Drives and Power Electronics* (pp. 1-6). IEEE. Quanzhou, China. https://doi.org/10.1109/precede.2019.8753329.

Geyer, T. (2017). *Model predictive control of high power converters and industrial drives*. John Wiley & Sons, United Kingdom.

Ghosh, S., Swarnkar, P., & Deshpande, D.M. (2019). Comparative analysis based on simulation & design aspects of three phase four switch inverter for industrial applications. *International Journal of Mathematical, Engineering and Management Sciences*, *4*(6), 1325-1340. https://dx.doi.org/10.33889/ijmems.2019.4.6-104.

Guazzelli, P.R.U., de Andrade Pereira, W.C., de Oliveira, C.M.R., de Castro, A.G., & de Aguiar, M.L. (2019). Weighting factors optimization of predictive torque control of induction motor by multiobjective genetic algorithm. *IEEE Transactions on Power Electronics*, *34*(7), 6628-6638. https://doi.org/10.1109/tpel.2018.2834304.

Harbi, I., Rodriguez, J., Liegmann, E., Makhamreh, H., Heldwein, M.L., Novak, M., Rossi, M., Abdelrahem, M., Trabelsi, M., Ahmed, M., Karamanakos, P., Xu, S., Dragicevic, T., & Kennel, R. (2023). Model-predictive control of multilevel inverters: Challenges, recent advances, and trends. *IEEE Transactions on Power Electronics*, *38*(9), 10845-10868. https://doi.org/10.1109/tpel.2023.3288499.

Kang, J.W., & Sul, S.K. (2001). Analysis and prediction of inverter switching frequency in direct torque control of induction machine based on hysteresis bands and machine parameters. *IEEE Transactions on Industrial Electronics, 48*(3), 545-553. https://doi.org/10.1109/41.925581.

Mahsahirun, S.N., Idris, N.R.N., Yusof, Z.M., & Sutikno, T. (2020). Fundamental elements of constant volt/hertz induction motor drives based on dSPACE DS1104 controller. *International Journal of Power Electronics and Drive System, 11*(4), 1670-1685. https://doi.org/10.11591/ijpeds.v11.i4.

Mamdouh, M., & Abido, M.A. (2019). Efficient predictive torque control for induction motor drive. *IEEE Transactions on Industrial Electronics*, *66*(9), 6757-6767. https://doi.org/10.1109/tie.2018.2879283.

Miranda, H., Cortés, P., Yuz, J.I., & Rodríguez, J. (2009). Predictive torque control of induction machines based on state-space models. *IEEE Transactions on Industrial Electronics, 56*(6), 1916-1924. https://doi.org/10.1109/tie.2009.2014904.

Mousavi, M.S., Davari, S.A., Nekoukar, V., Garcia, C., & Rodriguez, J. (2021). A robust torque and flux prediction model by a modified disturbance rejection method for finite-set model-predictive control of induction motor. *IEEE Transactions on Power Electronics*, *36*(8), 9322-9333. https://doi.org/10.1109/tpel.2021.3054242.

Muddineni, V.P., Bonala, A.K., & Sandepudi, S.R. (2016). Enhanced weighting factor selection for predictive torque control of induction motor drive based on VIKOR method. *IET Electric Power Applications*, *10*(9), 877-888. https://doi.org/10.1049/iet-epa.2016.0057.

Muddineni, V.P., Sandepudi, S.R., & Bonala, A.K. (2017). Finite control set predictive torque control for induction motor drive with simplified weighting factor selection using TOPSIS method. *IET Electric Power Applications, 11*(5), 749-760. https://doi.org/10.1049/iet-epa.2016.0503.

Novak, M., Xie, H., Dragicevic, T., Wang, F., Rodriguez, J., & Blaabjerg, F. (2021). Optimal cost function parameter design in predictive torque control (PTC) using artificial neural networks (ANN). *IEEE Transactions on Industrial Electronics*, *68*(8), 7309-7319. https://doi.org/10.1109/tie.2020.3009607.

Peter, A.K., Mathew, J., & Gopakumar, K. (2023). A simplified DTC-SVPWM scheme for induction motor drives using a single PI controller. *IEEE Transactions on Power Electronics, 38*(1), 750-761. https://doi.org/ 10.1109/tpel.2022.3197362.

Ravi Eswar, K.M., Kumar, K.V.P, & Kumar, T.V. (2018). Enhanced predictive torque control with auto-tuning feature for induction motor drive. *Electric Power Components and Systems, 46*(7), 825-836. https://doi.org/10.1080/15325008.2018.1509157.

Rodriguez, J., & Cortés, P. (2012). *Predictive control of power converters and electrical drives*. John Wiley & Sons, United Kingdom.

Rojas, C.A., Kouro, S., Perez, M., & Villarroel, F. (2015a). Multiobjective fuzzy predictive torque control of an induction machine fed by a 3L-NPC inverter. In *2015 IEEE International Symposium on Predictive Control of Electrical Drives and Power Electronics* (pp. 21-26). IEEE. Valparaiso, Chile.

Rojas, C.A., Rodriguez, J., Villarroel, F., Espinoza, J., & Khaburi, D.A. (2015b). Multiobjective fuzzy predictive torque control of an induction motor drive. In *The 6th Power Electronics, Drive Systems & Technologies Conference* (pp. 201-206). IEEE. Tehran, Iran. https://doi.org/10.1109/pedstc.2015.7093274.

Rojas, C.A., Rodriguez, J., Villarroel, F., Espinoza, J.R., Silva, C.A., & Trincado, M. (2013). Predictive torque and flux control without weighting factors. *IEEE Transactions on Industrial Electronics, 60*(2), 681-690. https://doi.org/10.1109/tie.2012.2206344.

Tang, L., Xu, W., Tang, Y., Ge, J., Yang, K., Islam, M.R., Li, W., & Su, S. (2023). Model predictive thrust control for linear induction machine: A fuzzy optimization approach. *IEEE Transactions on Industry Applications, 59*(2), 2532-2545. https://doi.org/10.1109/tia.2022.3225513.

Tang, L., Xu, W., Wang, X., Dong, D., Xiao, X., & Zhang, Y. (2021). Weighting factors optimization of model predictive control based on fuzzy thrust constraints for linear induction machine. *IEEE Transactions on Applied Superconductivity, 31*(8), 1-5. https://doi.org/10.1109/tasc.2021.3103704.

Trzynadlowski, A.M. (2000). *Control of induction motors*. Elsevier Science, USA. ISBN: 9780127015101, 9780127015108.

Trzynadlowski, A.M. (2013). *The field orientation principle in control of induction motors*. Springer Science & Business Media, US. ISBN: 9781461527305, 9781461527309.

Vazquez, S., Marino, D., Zafra, E., Peña, M.D.V., Rodríguez-Andina, J.J., Franquelo, L.G., & Manic, M. (2022). An artificial intelligence approach for real-time tuning of weighting factors in FCS-MPC for power converters. *IEEE Transactions on Industrial Electronics, 69*(12), 11987-11998. https://doi.org/10.1109/tie.2021.3127046.

Vazquez, S., Rodriguez, J., Rivera, M., Franquelo, L.G., & Norambuena, M. (2016). Model predictive control for power converters and drives: Advances and trends. *IEEE Transactions on Industrial Electronics, 64*(2), 935-947. https://doi.org/10.1109/tie.2016.2625238.

Vujji, A., & Dahiya, R. (2022). Experimental evaluation of VIKOR-based cost function optimization of finite control set-predictive torque control for permanent magnet synchronous motor drive. *Journal of Failure Analysis and Prevention, 22*(3), 1236-1251. https://doi.org/10.1007/s11668-022-01421-w.

Wang, F., Xie, H., Chen, Q., Davari, S.A., Rodriguez, J., & Kennel, R. (2019). Parallel predictive torque control for induction machines without weighting factors. *IEEE Transactions on Power Electronics, 35*(2), 1779-1788. https://doi.org/10.1109/tpel.2019.2922312.

Wang, X., Wang, Z., Xu, Z., Cheng, M., & Hu, Y. (2020). Optimization of torque tracking performance for direct-torque-controlled PMSM drives with composite torque regulator. *IEEE Transactions on Industrial Electronics, 67*(12), 10095-10108. https://doi.org/10.1109/tie.2019.2962451.

Zanchetta, P. (2011). Heuristic multi-objective optimization for cost function weights selection in finite states model predictive control. In *2011 Workshop on Predictive Control of Electrical Drives and Power Electronics* (pp. 70-75). IEEE. Munich, Germany. https://doi.org/10.1109/precede.2011.6078690.

Zhang, Y., & Yang, H. (2016). Two-vector-based model predictive torque control without weighting factors for induction motor drives. *IEEE Transactions on Power Electronics, 31*(2), 1381-1390. https://doi.org/10.1109/tpel.2015.2416207.

Zhong, L., Rahman, M.F., Hu, W.Y., & Lim, K.W. (1997). Analysis of direct torque control in permanent magnet synchronous motor drives. *IEEE Transactions on Power Electronics, 12*(3), 528-536. https://doi.org/10.1109/63.575680.

Publisher's Note- Ram Arti Publishers remains neutral regarding jurisdictional claims in published maps and institutional affiliations.